

18. METAMORPHISM OF CALC-SILICATE ROCKS FROM THE ALBORAN BASEMENT¹

Vicente López Sánchez-Vizcaíno² and Juan I. Soto³

ABSTRACT

Calc-silicate rocks are found in the high-grade metapelitic sequence of the Alboran Sea basement, drilled at Site 976 during Ocean Drilling Program Leg 161. These rocks occur as reaction zones, millimeters to several centimeters thick, along the contact between the marble and metapelite layers, and are interpreted as having been formed by diffusion processes between the two lithologies. Two different groups of calc-silicate rocks are distinguished according to the presence of garnet or scapolite. The garnet-bearing rocks display several reaction zones from the marble (Zone VII: calcite + quartz + plagioclase) to the metapelite (Zone I: biotite + corundum + plagioclase + K-feldspar + spinel; and Zone II: biotite + almandine-rich garnet + plagioclase + K-feldspar + quartz). The calc-silicate reaction zones are characterized by the appearance or disappearance of key mineral assemblages: appearance of pargasitic amphibole + biotite in Zone III, disappearance of biotite in Zone IV, appearance of clinopyroxene in Zone V, and appearance of grossular-rich garnet in Zone VI. Garnet and clinopyroxene break down to anorthite and actinolitic amphibole, respectively, which defines a secondary assemblage. Phase-relationship analysis suggests P-X_{CO2} peak conditions of 7.4–8.2 kbar and X_{CO2} = 0.11–0.16 for an assumed temperature of 650°C. The secondary growth of amphibole and plagioclase probably occurred under decreasing pressure and increasing X_{CO2} conditions. Scapolite-bearing assemblages in calc-silicate rocks indicate minimum temperatures of 550–600°C.

INTRODUCTION

The Alboran Sea, in the western Mediterranean, is one of several extensional basins of late Tertiary age that formed in close association with the compressional orogens comprising the Alpine system. The Alboran Sea is partly surrounded by an arcuate mountain chain formed by the Betic (southern Spain) and the Maghrebian Chains (Rif and Tell, in Morocco; Fig. 1). Within these mountain chains, contractional deformation continued during basin formation. The Alboran Sea in fact appears to have formed on the extended and thinned remnants of a late Mesozoic–Paleogene orogen (known as the Alboran Domain) that forms the Internal Zones of the surrounding mountain chains (Fig. 1). During the Neogene evolution of the basin, contraction continued in the External Betic and Rif belts to form the present arcuate structure (Platt and Vissers, 1989; Comas et al., 1992; García-Dueñas et al., 1992).

One of the objectives of Ocean Drilling Program (ODP) Leg 161 was to investigate the basement of the Alboran Sea basin, as its nature, structural history, and thermal evolution contain evidence useful for constructing satisfactory rifting models for the region, and to test various tectonic hypotheses (see Comas, Zahn, Klaus, et al., 1996). To allow substantial penetration of the acoustic basement, Site 976 was located on a basement high (Fig. 1), covered by a thin, discontinuous sedimentary sequence, middle Miocene through Pliocene–Pleistocene in age (Shipboard Scientific Party, 1996). This basement high is ~50 km long and 15 km wide, and was partially drilled during Leg 13 at Deep Sea Drilling Project (DSDP) Site 121 (Shipboard Scientific Party, 1973). The orientation of this basement high changes southward from northeast–southwest at Site 976, to north–northwest–south–southeast. Interpretation of multichannel commercial seismic profiles indicates that this basement elevation corresponds to a horst limited by north–south and northeast–southwest–trending normal faults, which bound a major depocenter with up to 8 km of lower Miocene–Pleistocene sedi-

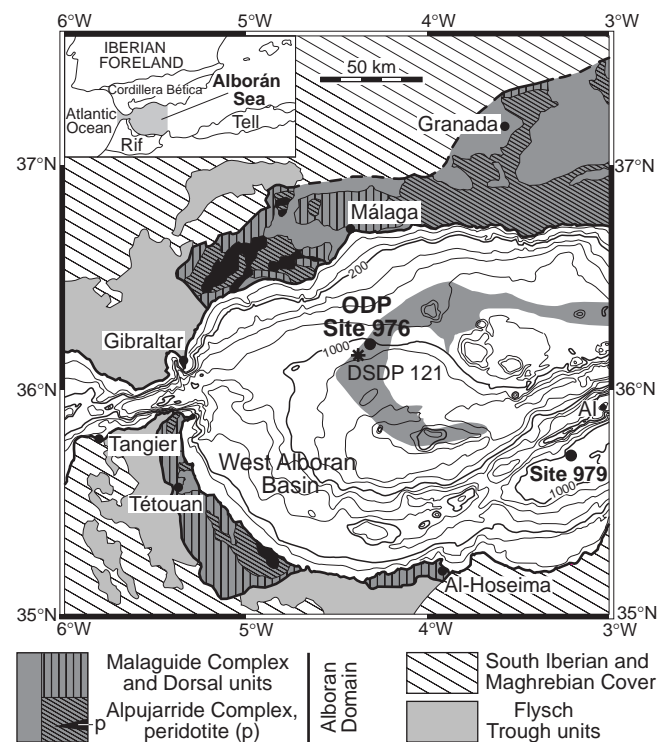


Figure 1. Location of Sites 976 and 121 in the western Alboran Sea basin and simplified geologic map of the surrounding Betic and Rif mountain belts. Bathymetric contours are every 200 m; each latitude grade equals 111 km (from Comas et al., 1993).

tions toward the west (Comas et al., 1992; Watts et al., 1993; de la Linde et al., 1996; Soto et al., 1996).

During Leg 161, the *JOIDES Resolution* drilled into the acoustic basement at Site 976 (Holes 976B and 976E), penetrating and sampling 258.97 m (Hole 976B, 1108.0 m water depth, from 669.73 to 928.70 mbsf) and 84.22 m (Hole 976E, 1107.6 m water depth, from 652.08 to 736.30 mbsf) of metamorphic rocks. These rocks include

¹Zahn, R., Comas, M.C., and Klaus, A. (Eds.), 1999. *Proc. ODP, Sci. Results*, 161: College Station, TX (Ocean Drilling Program).

²Departamento de Geología, Universidad de Jaén, Escuela Universitaria Politécnica de Linares, C/Alfonso X el Sabio 28, 23700 Linares, Spain. vlopez@ujaen.es

³Instituto Andaluz de Ciencias de la Tierra and Departamento de Geodinámica, C.S.I.C.-Universidad de Granada, 18071 Granada, Spain.

high-grade pelitic schist, pelitic gneiss, migmatite, and granite dikes, together with minor amounts of marble and calc-silicate rocks (Shipboard Scientific Party, 1996; Fig. 2).

This paper reports the main results of post-cruise petrologic studies of calc-silicate rocks from basement samples recovered at Site 976 (Holes 976B and 976E). The characterization of the principal stages of their metamorphic evolution in terms of changes in the intensive variables pressure (P), temperature (T), and composition of the fluid ($X_{\text{CO}_2} = \text{CO}_2/[\text{CO}_2 + \text{H}_2\text{O}]$) are based on (1) the detailed petrographic study of 22 selected samples; (2) the characterization of mineral chemistry by microprobe analyses; and (3) the calculation of a phase diagram that models phase and textural relationships.

Calc-silicate rocks occur as bands along the contact between marbles and metapelites; thus, they can be interpreted as reaction zones formed by diffusion metasomatic processes, such as those described by Brady (1977) and Joesten (1977; 1991). These bands are characterized by the development of separate zones with different high-variance mineral assemblages. The application of the phase rule to these chemical open systems and the determination of the stability conditions of the mineral assemblages assume local equilibrium (Thompson, 1959).

In this paper, several terms are used to refer to metacarbonate rocks and carbonate-bearing mineral assemblages. The term marble is used to designate a metacarbonate rock in which calcite and/or dolomite predominate over all other mineral classes (silicates, oxides, sulfides, etc.). Therefore, the term calc-silicate rock refers to a lithology in which, independently of texture or formation process, Ca-rich silicates are more abundant than carbonates (calcite, in this case).

MACROSCOPIC DESCRIPTION OF CALC-SILICATE ROCKS

The occurrence of marbles and calc-silicate rocks varies in Holes 976B and 976E. In Hole 976B, they appear as scarce intercalations, usually only a few centimeters thick, within the high-grade schists that form the upper part of the basement section (Fig. 2; Shipboard Scientific Party, 1996). In Hole 976E, the proportion of metacarbonate rocks is higher (Fig. 2), in part because the hole followed the dip of a marble layer (Shipboard Scientific Party, 1996; fig. 54).

Dolomite marbles are pale green, gray, white, or yellow, commonly associated with zones of brecciation and faulting, especially in Hole 976B (interval 161-976B-102R-1 [Pieces 7 and 8, 58–70 cm]). Calcite marbles occur as gray to greenish layers that alternate with high-grade schists and calc-silicate rocks (Fig. 2). Their thickness ranges from several centimeters to, exceptionally, one meter (interval 976E-13R-3 [Pieces 10–14, 72–150 cm]). The marble fabric is characterized by weak (e.g., interval 976B-81R-2 [Pieces 6–8, 58–81 cm]) to strong banding (e.g., Sample 976E-13R-3 [Pieces 8 and 9, 50–63 cm]) that defines the foliation of the rocks, and is commonly folded by isoclinal folds (e.g., Sample 976B-83R-2 [Piece 1, 0–13 cm]). The banding is characterized by the alternation of carbonate-rich zones (several millimeters to several centimeters thick) with metapelite and/or calc-silicate layers (e.g., interval 976E-15R-1 [Pieces 5–6]).

Calc-silicate rocks appear most commonly as green reaction zones along the contact between the marble and metapelite layers. The morphology and thickness of these bands varies extensively. They occur as bands, 1–6 mm thick (e.g., interval 161-976E-14R-1 [Pieces 2 and 3A, 10–40 cm]), with sharp contacts with the marble and metapelite layers. The bands consist of elongated grains of clinopyroxene (Sample 976E-15R-1 [Piece 5, 37–88 cm]) and amphibole (Sample 976E-15R-2 [Piece 6, 53–57 cm]), massive (Sample 976E-13R-3 [Piece 8, 50–63 cm]) or scattered garnets (Sample 976E-13R-3 [Piece 14, 137–150 cm]), and pyrite crystals (Sample 976E-13R-3 [Piece 1, 0–15 cm]). The reaction zones are parallel to the main foliation (S_2 ; Shipboard Scientific Party, 1996) and in many cases are folded with it (interval 976E-15R-2 [Pieces 8–13, 66–118

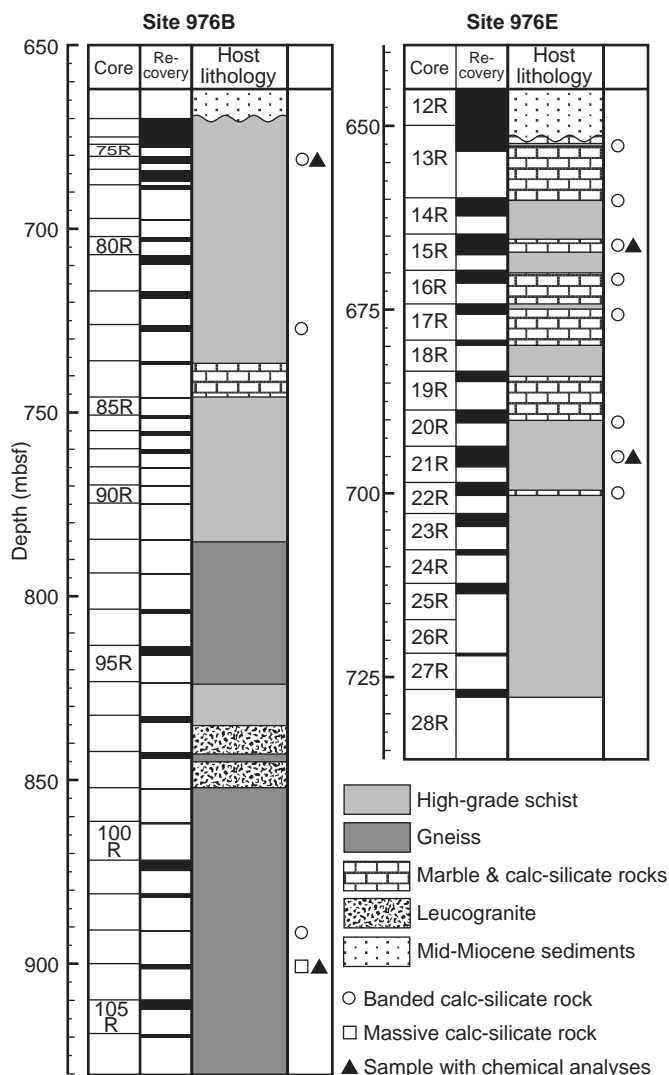


Figure 2. Lithologic columns of basement at Holes 976B and 976E with the location of the studied samples of calc-silicate rocks.

cm]). Gradational contacts between calc-silicate rocks and marble and schists were also observed, and are especially abundant in strongly deformed rocks (Sample 976E-17R-1 [Piece 5, 57–67 cm]), where calc-silicate bands may have a very irregular shape and variable thickness (up to several centimeters; e.g., Sample 976E-21R-3 [Piece 1, 0–47 cm]; Fig. 3A). These bands can include transposed fragments of pelites (Sample 976E-20R-1 [Piece 11, 61–95 cm]). Alteration processes have greatly modified the appearance of the calc-silicate rocks, as illustrated in Figure 3B (Sample 976B-104R-1 [Pieces 8–14, 57–125 cm]). Altered calc-silicate rocks are thick (up to 80 cm), massive, and mottled in aspect, comprising large aggregates (up to 7 cm long) of pale plagioclase crystals surrounded by a dark green, highly altered granular matrix (Fig. 3B).

Pale green calc-silicate rocks also occur intercalated with gneiss in the lower part of Hole 976B (Fig. 2), with no evident associated marble bands (Sample 161-976B-103R-1 [Piece 10, 45–57 cm]).

Textural Relationships and Mineral Assemblages

We examined 22 thin sections of marble and calc-silicate rocks, seven from Hole 976B and 15 from Hole 976E (see location in Fig. 2).

Detailed microscopic study shows that calc-silicate rocks normally appear as 0.5- to 2.25-mm thick, mineralogically simple, reaction

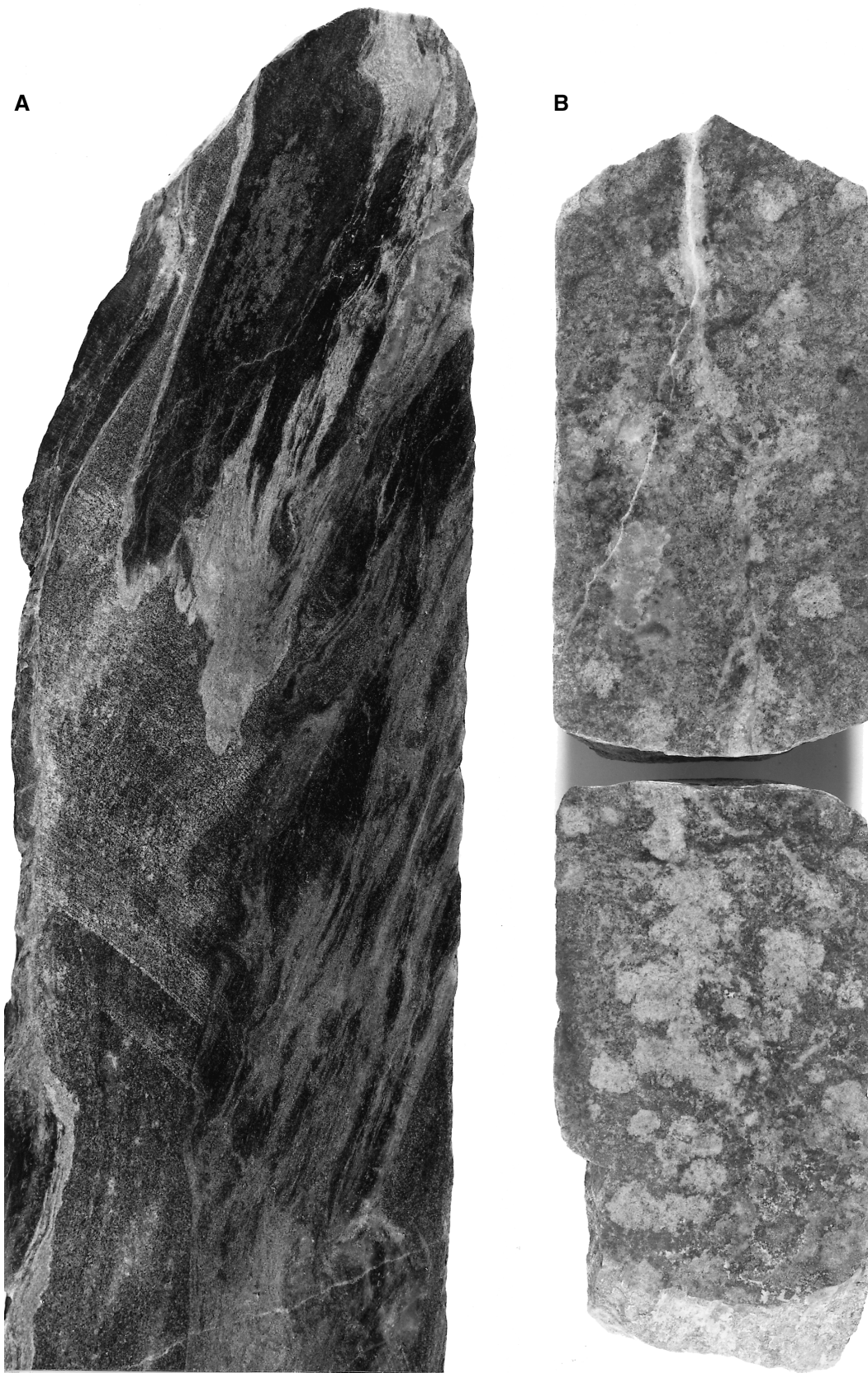


Figure 3. Core photographs of (A) banded (Sample 161-976E-15R-1 [Piece 6A, 89–105 cm]) and (B) massive (Sample 161-976B-104R-1 [Pieces 10 and 11, 77–105 cm]) calc-silicate rocks.

zones along the contact between carbonate and quartz-feldspar rich metapelite layers. They also occur within marble or metapelite layers, related to the presence of quartz-feldspar aggregates or to carbonate, respectively. These simple reaction zones consist essentially of prismatic, and less commonly, rounded, slightly green crystals of clinopyroxene oriented parallel to the marble-metapelite contact (Pl. 1, fig. 1). Clinopyroxene grains vary in size from one sample to another and also within the same sample (the largest grains may be up to 3 mm long).

In other samples, however, calc-silicate rocks are characterized by the formation of several reaction zones with differences in their mineral compositions. These calc-silicate rocks can be divided into two groups according to the occurrence of grossular-rich garnet or scapolite. Garnet and scapolite never appear together in the same rock and the formation of one or another type of calc-silicate rock is probably controlled by differences in bulk-rock composition.

Garnet-Bearing Calc-Silicate Rocks

Garnet-bearing calc-silicate rocks appear as up to 0.5-cm-thick reaction zones between metapelite and marble layers. The most complete sequence of zones with a changing mineralogy was found in Sample 161-976B-76R-1 (Piece 9A, 66–87 cm). In this type of calc-silicate rock, several zones can be distinguished between the metapelite and the marble. These zones result from the interaction between an aluminum-rich metapelite, containing plagioclase, K-feldspar, biotite, spinel, and corundum (Zone I), and a calcite marble, containing quartz and plagioclase (Zone VII).

The mineralogic assemblages and the compositional variation of minerals from the different calc-silicate zones define several fields in an ACF projection (Fig. 4), where $A = \text{Al}_2\text{O}_3 + \text{Fe}_2\text{O}_3$; $C = \text{CaO}$; $F = \text{FeO} + \text{MgO}$. Zone II is characterized by the disappearance of spinel and corundum (present in Zone I) and the appearance of subidioblastic porphyroblasts of almandine-rich garnet. Zone III is formed by pargasitic amphibole in equilibrium with biotite and garnet. Zone IV is defined by the disappearance of biotite and the ubiquitous occurrence of amphibole as bands with a nematoblastic texture. In Zone V, amphibole and garnet disappear, and small grains of clinopyroxene form a granoblastic aggregate. This zone is not always present, and Zone IV can also be found directly in contact with Zone VI. The latter zone, directly in contact with the calcite marble (Zone VII), consists of coarse-grained clinopyroxene and occasionally grossular-rich garnet (Pl. 1, fig. 3). Titanite (up to 0.9 mm) and pyrite commonly occur in Zone VI. Quartz and plagioclase are always present in Zones II–V.

The sequence of mineral assemblages from Zones III to VII can be found with minor differences in other samples. For example, grossular-rich garnet can occur as almost monomineral bands (up to 2.75 mm thick; Sample 161-976E-21R-1 [Piece 3, 27–31 cm]; Pl. 1, fig. 2). This garnet contains abundant inclusions of quartz, calcite, plagioclase, clinopyroxene, epidote, and titanite, oriented parallel to the external S_2 foliation. Garnet also has perpendicular veins filled with calcite, plagioclase, and opaque minerals (Pl. 1, fig. 2).

The primary calc-silicate assemblages may have been partially replaced by secondary minerals such as amphibole, plagioclase, and epidote. Light green actinolitic amphibole occurs, together with quartz and calcite, as the replacement product of clinopyroxene, which appears as relict inclusions within amphibole crystals (Pl. 2, fig. 1). In some rocks, large plagioclase grains, calcite, and quartz crystals surround small xenomorphic grains of grossular-rich garnet (Pl. 1, fig. 4). This texture suggests a breakdown reaction of garnet.

Epidote is also a minor constituent of garnet-bearing calc-silicate rocks. It may appear as secondary clinozoisite grains included in massive garnet bands and related to the previously described veins, or in contact with clinopyroxene, garnet, plagioclase, and titanite. Epidote also occurs as isolated grains or, more commonly, forming

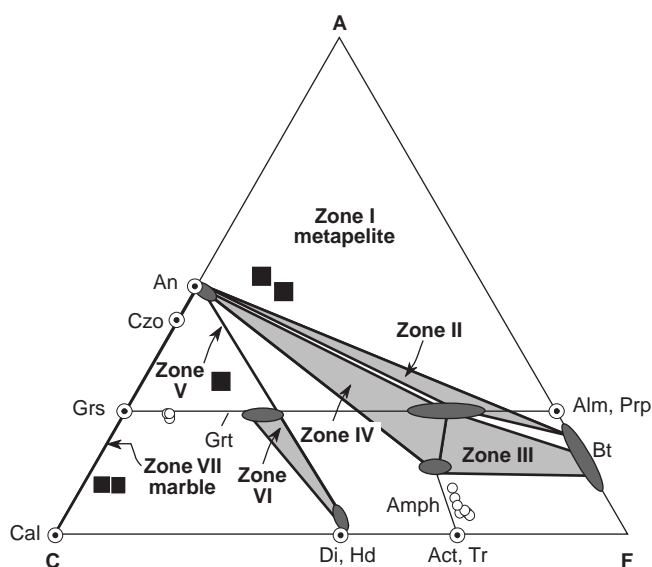


Figure 4. ACF diagram with the mineral assemblages from different reaction zones (light gray fields) found in Sample 161-976B-76R-1 (Piece 9A, 66–87 cm). Dark gray fields represent chemical analyses of minerals from reaction zones; open circles are chemical analyses from secondary amphibole and relics of garnet. Solid squares represent whole-rock analyses from metapelites and marbles. $A = \text{Al}_2\text{O}_3 + \text{Fe}_2\text{O}_3$; $C = \text{CaO}$; $F = \text{FeO} + \text{MgO}$; An = anorthite; Czo = clinozoisite; Grs = grossular; Cal = calcite; Grt = garnet; Amph = amphibole; Di = diopside; Hd = hedenbergite; Act = actinolite; Tr = tremolite; Alm = almandine; Prp = pyrope; Bt = biotite; mineral abbreviations are after Kretz (1983).

bands of radial aggregates within layers rich in quartz + feldspar, parallel to the contact between metapelite and marble bands. In both textural occurrences clinzoisite is surrounded by a narrow rim or cloud of fine-grained opaque minerals. Aggregates of fine-grained, highly birefringent epidote can also appear replacing, partially or completely, elongated grains of opaque minerals. Allanite also occurs in the core of zoned clinozoisites and as small rounded grains associated with large plagioclase crystals.

K-feldspar was recognized in most of the samples. In its most conspicuous form, K-feldspar appears as rounded or elongated grains of variable size, in contact with partially destabilized garnet and clinopyroxene grains. In Sample 161-976B-104R-1 (Piece 8, 59–65 cm), K-feldspar also occurs in veins that cut plagioclase porphyroblasts (Pl. 2, fig. 4).

Scapolite-Bearing Calc-Silicate Rocks

Scapolite-bearing calc-silicate rocks are less abundant than the garnet-bearing ones. Clinopyroxene, with textures similar to those previously described, remains the most common phase in these reaction zones. Scapolite usually occurs as poikiloblasts crowded with inclusions of clinopyroxene, quartz, titanite, and calcite (Pl. 2, fig. 2). Scapolite poikiloblasts appear in two different textural positions: as rounded grains (up to 2.5 mm) on the metapelitic side of reaction zones, and as large poikiloblasts (up to 7.5×1.5 mm) that form the main part of the rock. In the latter case, clinopyroxene inclusions, sometimes overgrown by amphibole in the border, can be partially or completely altered to a very fine-grained mass of chlorite, other sheet silicates, and calcite (Pl. 2, fig. 3). In both cases, scapolite and plagioclase abundance are inversely related. More rarely, small scapolite grains also appear in contact with clinopyroxene, plagioclase, and

amphibole, in contact with K-feldspar grains or even cut by veins of K-feldspar. Late, Na-rich plagioclase veins also appear in some scapolite-bearing rocks.

Mineral Chemistry

To characterize the mineral chemistry and its possible variation with textural positions, we selected seven samples for microprobe analyses. Their location in the lithologic column is presented in Figure 2.

These samples were analyzed using an electron microprobe (Cameca SX50) at the Universidad de Granada. An acceleration voltage of 15 kV, a beam current of 20 nA, and a beam diameter of 8 μm were used. Standards were both natural and synthetic substances. Data were reduced using the PAP procedure from Pouchou and Pichoir (1985). Representative analyses and chemical formulas of the minerals are shown in Table 1. Mineral and end-member abbreviations are after Kretz (1983).

Clinopyroxene

The chemical composition of clinopyroxene is essentially contained within the diopside-hedenbergite solid solution (Wo₄₅₋₅₀En₁₀₋₄₃Fs₂₋₃₈). A significant X_{Mg} variation is observed between different samples and also within the same sample. This might be related essentially to changes in the bulk-rock composition and in the mineralogical composition. Significant zoning patterns in single grains are rare, except for a slight Mg increase from core to rim.

Contents of other elements are always very low: Al_{total} < 0.08 ions per formula unit (pfu), Na < 0.02 pfu, Fe³⁺ < 0.05 pfu, and Mn < 0.03 pfu.

Garnet

The main garnet compositional trends are plotted in Figure 5, where four groups of data can be distinguished that correspond to different textural positions. Garnets from Zone VI, either those in contact with clinopyroxene or those forming massive bands, are rich in grossular and almandine, with significant amounts of andradite and spessartine (Grs₄₉₋₆₅ Alm₂₃₋₃₄ Adr_{2,8-12,3} Prp_{0,5-3,6} Sps_{2,6-6,5}). The reported chemical variations correspond to grains from different samples, whereas the composition of single grains is remarkably homogeneous. Relict garnets destabilized to secondary plagioclase have a granditic composition (Grs_{64,3-73} Alm_{0-0,8} Adr₂₄₋₃₃ Prp_{0,3-0,4} Sps_{2-2,5}). Small xenoblastic relict garnet preserved within the late retrogressive mass has a grossular-rich and almandine-poor composition (Grs_{79-80,5} Alm_{7,7-8,8} Adr_{8,8-10,7} Prp_{0,2} Sps_{1,6-2,2}). Garnet from Zones II, III, and IV is richer in almandine, pyrope, and spessartine (Grs_{14,84-32,6} Alm_{53,5-68,5} Adr_{0-2,6} Prp_{4,6-7,4} Sps_{7-11,2}) than any other garnet group.

Plagioclase

Plagioclase from garnet-bearing calc-silicate rocks has a homogeneous chemical composition, near pure anorthite (An₉₃₋₉₉). In contrast, plagioclase from scapolite-bearing assemblages may have higher Na contents (An₇₈₋₉₉). In these rocks, late plagioclase veins that cut previous assemblages have a labradorite composition (An₆₀₋₇₀).

Amphibole

All the studied amphiboles can be classified as calcic amphiboles (after Leake, 1978). The two most important exchange vectors explaining their chemical composition, choosing tremolite as the addi-

Table 1. Representative mineral analyses and formulae.

| Mineral: | Clinopyroxene | Garnet | Garnet | Plagioclase | Amphibole | Scapolite | Clinozoisite | Titanite |
|--|-----------------------------|-------------------------|-------------------------|---------------------------|---|---------------------------|-------------------------|-----------------------------|
| Sample: | 161-976B-76R-1, 72-75 cm | 976B-76R-1, 72-75 cm | 976B-104R-1, 9-62 cm | 976B-76R-2, 116-119 cm | 976B-76R-1, 72-75 cm | 976E-15R-1, 126-128 cm | 976E-21R-3, 27-31 cm | 976B-76R-2, 116-119 cm |
| I: | Cpx6-5 | Grt3-2 | Grt4-1 | Pl1-4 | Amph2-6 | Scp1-5 | Czo3-5 | Ttn2-3 |
| SiO ₂ | 50.21 | 38.74 | 38.42 | 43.43 | 46.35 | 45.51 | 38.65 | 30.25 |
| TiO ₂ | 0.08 | 0.14 | 0.33 | 0.00 | 0.27 | 0.01 | 0.14 | 36.84 |
| Cr ₂ O ₃ | 0.03 | 0.02 | 0.06 | 0.01 | 0.05 | 0.00 | 0.00 | 0.01 |
| Al ₂ O ₃ | 0.74 | 19.81 | 16.03 | 36.04 | 6.54 | 27.56 | 26.56 | 2.58 |
| FeO | 20.31 | 13.55 | 8.18 | 0.22 | 26.69 | 0.20 | 9.10† | 0.56† |
| MnO | 0.77 | 2.96 | 0.98 | 0.03 | 0.74 | 0.01 | 0.13 | 0.02 |
| MgO | 5.12 | 0.23 | 0.08 | 0.00 | 4.92 | 0.00 | 0.02 | 0.01 |
| CaO | 22.82 | 24.58 | 35.58 | 20.22 | 11.06 | 19.05 | 23.97 | 29.22 |
| Na ₂ O | 0.06 | 0.00 | 0.00 | 0.12 | 0.35 | 2.66 | 0.00 | 0.00 |
| K ₂ O | 0.00 | 0.00 | 0.01 | 0.01 | 0.23 | 0.18 | 0.00 | 0.00 |
| Cl | n.a. | n.a. | n.a. | n.a. | n.a. | 0.10 | n.a. | n.a. |
| Total | 100.15 | 100.26 | 100.58 | 100.09 | 97.34 | 95.28 | 98.55 | 99.49 |
| O = Cl | 0.00 | 0.00 | 0.00 | 0.00 | 0.00 | 0.02 | 0.00 | 0.00 |
| Total | 100.15 | 100.26 | 100.58 | 100.09 | 97.34 | 95.26 | 98.55 | 99.49 |
| | Wood and Banno (1973) | 8 cat - 12 O | | 5 cat - 8 O | cat - Na - K = 15 | Si + Al = 12 | 12 cat + OH | 3 cat - 5 O |
| Si | 1.988 | 3.017 | 2.969 | 2.010 | 7.210 | 7.001 | 3.008 | 0.978 |
| Ti | 0.002 | 0.009 | 0.019 | 0.000 | 0.032 | 0.001 | 0.008 | 0.896 |
| Al ^{iv} | 0.012 | 0.000 | 0.031 | 0.000 | 0.790 | 0.000 | 0.000 | 0.000 |
| Al ^{vi} | 0.023 | 1.818 | 1.429 | 1.966 | 0.409 | 4.999 | 2.437 | 0.098 |
| Cr | 0.001 | 0.001 | 0.004 | 0.001 | 0.006 | 0.000 | 0.000 | 0.000 |
| Fe ³⁺ | 0.000 | 0.131 | 0.528 | 0.008 | 0.159 | 0.000 | 0.533 | 0.014 |
| Fe ²⁺ | 0.673 | 0.752 | 0.000 | 0.000 | 3.313 | 0.026 | 0.000 | 0.000 |
| Mn | 0.026 | 0.195 | 0.064 | 0.001 | 0.097 | 0.001 | 0.008 | 0.001 |
| Mg | 0.302 | 0.027 | 0.009 | 0.000 | 1.141 | 0.001 | 0.002 | 0.001 |
| Ca | 0.968 | 2.051 | 2.945 | 1.003 | 1.843 | 3.141 | 1.999 | 1.013 |
| Na | 0.005 | 0.000 | 0.000 | 0.011 | 0.105†† | 0.793 | 0.000 | 0.000 |
| K | 0.000 | 0.000 | 0.001 | 0.000 | 0.046 | 0.036 | 0.000 | 0.000 |
| Cl | n.a. | n.a. | n.a. | n.a. | n.a. | 0.027 | n.a. | n.a. |
| Compositional parameters and end members | | | | | | | | |
| | Wo = 0.479 | Grs = 0.61 | Grs = 0.70 | An = 0.99 | Tsch = 0.64 | EqAn = 66.62 | Czo = 0.45 | CaTiSiO ₅ = 0.91 |
| | En = 0.151 | Alm = 0.25 | Alm = 0.00 | | Fe ³⁺ - Al ^{vi} = 0.249 | | | |
| | Fs = 0.336 | Prp = 0.01 | Prp = 0.00 | | Ed = 0.15 | | | |
| | | Sps = 0.07 | Sps = 0.02 | | K - Na(A) = 0.30 | | | |
| | | Adr = 0.07 | Adr = 0.26 | | Fe ²⁺ - Mg = 0.73 | | | |

Note: n.a. = not analyzed, † = iron as Fe₂O₃, †† = all Na in site A, cat = cation. Mineral abbreviations are after Kretz (1983).

tive component (Thompson, 1981), are the tschermak and edenite vectors (Fig. 6). The value of both vectors increases from secondary amphiboles replacing clinopyroxene, or those in contact with scapolite, toward those growing in Zones III and IV. The value of exchange vector $FeMg_{-1}$ is always high (up to 0.73), but the extent of this substitution is very homogeneous within each sample, which could be determined by local bulk composition. KNa_{-1} exchange vector in site A is important in both amphiboles from Zones III and IV (up to 0.57) and secondary amphiboles (up to 0.40). In Zones III and IV, however, the differences between one sample and another are great than in secondary amphiboles. Substitution of Fe^{3+} for Al in octahedral sites shows a wide variation (0.132–0.364) in the amphiboles. Finally, the $MgCa_{-1}$ vector in site M4 may be significant (up to 0.239), and the changes are once again important between one sample and another.

Scapolite

The chemical composition of scapolite is represented in a conventional EqAn- X_{Cl} diagram (Fig. 7), where EqAn are equivalents of anorthite ($[Al - 3]/3$) and $X_{Cl} = (Cl/[Cl + CO_3])$. The values for the studied scapolites (EqAn = 61.3%–69.2% and $X_{Cl} < 0.05$) are very close to those of mizzonite (67% EqAn and $X_{Cl} = 0$), one of the three end-members that define the scapolite solid solution. SO_3 and F contents in scapolite are negligible (Table 1). K_2O values are very low (0.12–0.32 wt%). The sum of $Ca + Na + K$ is, in most cases ~ 3.9 pfu, which indicates a slight deficit in the site occupied by these cations that could in part result from Na evaporation during the analytical procedure.

No clear chemical differences can be observed in scapolites from different textural positions. Chemical variation within single crystals may reach 4.3% EqAn. In some grains, a core-to-rim EqAn enrichment can be appreciated.

Epidote

Clinozoisites are rich in Fe^{3+} (0.211–0.627 pfu), and individual samples show significant chemical variations. Some allanites also

have high contents of Fe^{3+} and rare-earth elements, especially Ce (around 10 wt%).

Titanite

Titanite has a homogeneous composition without differences between crystals of different grain size. Al_2O_3 (1.22–3.18 wt%) and Fe_2O_3 (0–0.81 wt%) contents are always low.

Origin of Reaction Zones

Many of the studied calc-silicate rocks, especially in the case of the garnet-bearing type, appear as clearly defined reaction zones with a mineral composition that evolves from metapelite to marble layers,

GARNET COMPOSITION

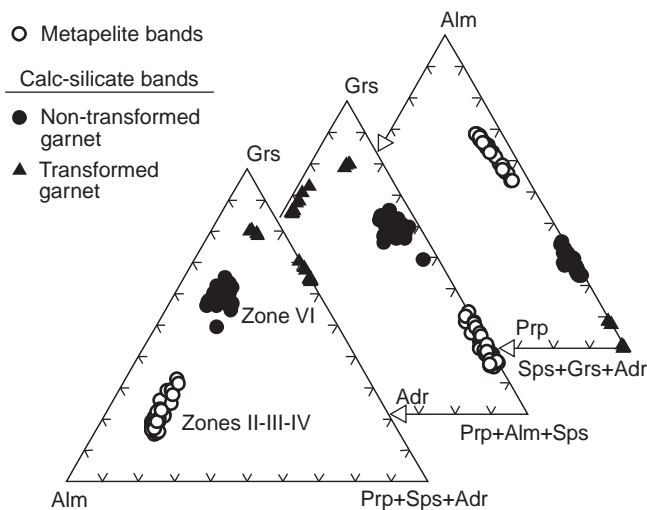


Figure 5. Garnet compositions in calc-silicate rocks for almandine (Alm), pyrope (Prp), grossular (Grs), spessartine (Sps), and andradite (Adr) components (mineral abbreviations after Kretz, 1983). Solid circles represent garnet grains in equilibrium with clinopyroxene in Zone VI; open circles represent garnet grains from Zones II, III and IV; triangles represent garnet grains partially transformed to plagioclase, calcite, and quartz.

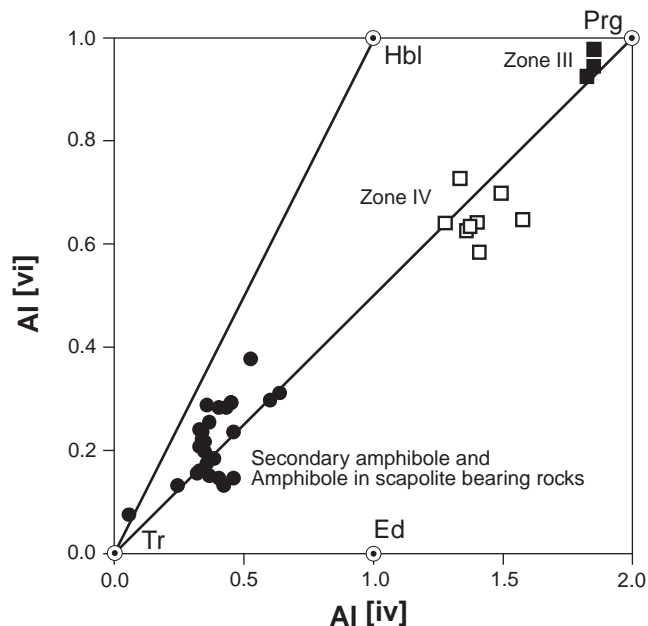


Figure 6. Chemical composition of amphibole expressed by the Al^{iv} vs. Al^{vi} variation. Solid squares represent the chemical composition of amphibole in Zone III, open squares represent the chemical composition of amphibole in Zone IV, and solid circles represent the chemical composition of secondary amphibole in garnet-bearing rocks and also the chemical composition of amphibole in scapolite-bearing calc-silicate rocks. Circles with dots represent the chemical composition of tremolite (Tr), edenite (Ed), hornblende (Hbl), and pargasite (Prg) end-members (mineral abbreviations after Kretz, 1983).

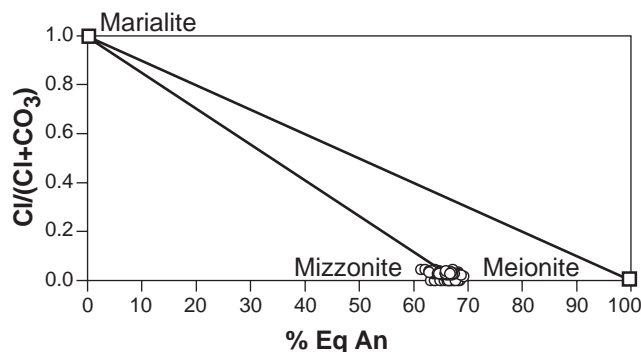


Figure 7. Chemical variation of scapolite expressed as EqAn (%) vs. $Cl/(Cl + CO_3)$, and the location of the end-members meionite, marialite, and mizzonite.

as represented in the ACF diagram from Figure 4. This sequence of zones is similar to those described in other calc-silicate reaction zones (e.g., Thompson, 1975; Kerrick, 1977).

These reaction zones are characterized by sharp boundaries and a low number of phases that are stable in each zone; their formation could be controlled by diffusional processes determined by chemical potential gradients (Joesten, 1977). Another possible origin for the reaction zones, suggested for other calc-silicate rocks, is infiltration. For the calc-silicate rocks examined here, however, several arguments suggest a limited influence of this factor. First, because metamorphic rocks have low porosity (Brady, 1977), fluid circulation would be restricted, producing small-scale reaction bands. Second, infiltration processes could not generate a symmetric distribution of calc-silicate bands from metapelite to marble on both sides of the metapelite intercalations (e.g., Sample 161-976E-21R-1 [Piece 3, 27–31 cm]). Finally, if infiltration were involved in the generation of these calc-silicate rocks, it would produce a larger variation in the chemical composition of the minerals (Thompson, 1975) compared with the data presented here.

From the ACF diagram (Fig. 4) it can be deduced that the formation of the represented mineral assemblages occurred because of an increase in the chemical potential (μ) of CaO from pelite to marble, balanced by diffusion of Al_2O_3 in the opposite direction. The occurrence of quartz in all the reported zones indicates that μ_{SiO_2} remained constant during this process. Furthermore, calculations of $\mu_{\text{CaO}}\text{-X}_{\text{CO}_2}$ diagrams, at constant P and T deduced from Figure 8 (see next section), support the hypothesis of CaO diffusion as the main factor controlling the formation of the reported reaction zones in the garnet-bearing calc-silicate rocks. Preliminary results show, in fact, that the assemblage amphibole + biotite + plagioclase (Zone III in Fig. 4) is stable at lower μ_{CaO} values than the assemblage clinopyroxene + garnet (Zone VI).

Phase Relationships and Metamorphic Conditions

The analysis of phase relationships of the calc-silicate assemblages and the estimation of P-T- X_{CO_2} conditions at which they were formed are subject to the following initial constraints: (1) the ambiguous textural relationships of amphibole and scapolite in scapolite-bearing reaction zones; (2) the typical high thermodynamic variance of most mineral assemblages occurring in metasomatic reaction zones (Joesten 1991); (3) the complexity of the chemical system of the rocks ($\text{SiO}_2\text{-Al}_2\text{O}_3\text{-CaO-Na}_2\text{O-K}_2\text{O-FeO-MgO-Fe}_2\text{O}_3\text{-TiO}_2\text{-CO}_2\text{-H}_2\text{O}$) and the complex composition of some minerals, such as garnet and amphibole; and (4) the lack of reliable thermodynamic data for some end-members that could be required for the total description of the observed solid solutions (mizzonite in scapolite and many amphibole end-members).

With these uncertainties in mind, we first assumed that local equilibrium exists in the contact between mineral assemblages from adjacent zones (Thompson, 1959; Joesten 1977). The principle of local equilibrium was then applied to the calculation of the P-T- X_{CO_2} stability conditions from the low-variance assemblage clinopyroxene + grossular-rich garnet + amphibole + anorthite + quartz + calcite, which occurs in the observed contact between Zones IV and VI in Sample 161-976B-76R-1 (Piece 9A, 66–87 cm). Metamorphic conditions for the subsequent formation of secondary actinolitic amphibole were also estimated here.

To this end, we simplified the chemical composition of the minerals and the solid-solution models used in our calculation of phase relationships and metamorphic conditions. We considered amphibole as an ideal solid solution between the tremolite, ferrotremolite, pargasite, and ferropargasite end-members (see Fig. 6). We also used the garnet solid-solution model of Berman (1990) between the grossular, pyrope, and almandine end-members, and the solid-solution model of

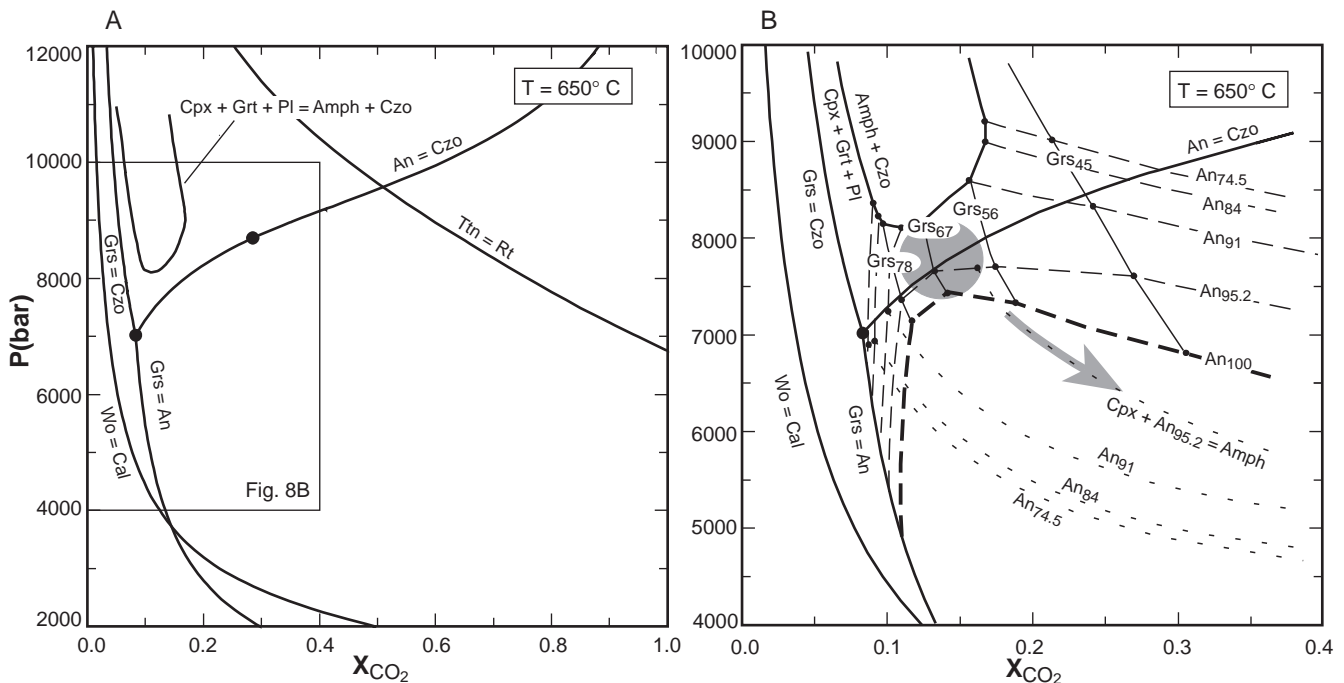


Figure 8. P- X_{CO_2} projection at constant $T = 650^\circ\text{C}$, in the system $\text{Al}_2\text{O}_3\text{-FeO-MgO-Na}_2\text{O}$, after projection through SiO_2 and CaO. **A.** Univariant reactions (thick solid lines) and invariant points (solid circles). **B.** Enlarged portion of diagram in A shows the phase relationships and stability conditions of the assemblage clinopyroxene + grossular-rich garnet + amphibole + anorthite + quartz + calcite (shaded field) and of the breakdown reaction of clinopyroxene to produce amphibole in the presence of anorthite-rich plagioclase (shaded arrow). Thick solid lines represent univariant reactions, long dashed lines contour the anorthite content in plagioclase, thin solid lines contour the grossular content in garnet, and dotted lines represent the conditions of clinopyroxene reacting to amphibole for different anorthite contents in plagioclase. Minerals on the right side of the reactions are stable at high-pressure conditions. Mineral abbreviations are after Kretz (1983).

anorthite-rich plagioclase of Newton et al. (1980). Finally, we considered clinozoisite, titanite, rutile, wollastonite, calcite, and quartz to be pure phases. All the mineral thermodynamic data are from the data base of Holland and Powell (1990, modified unpubl. data, 1994).

Additional constraints in our calculations are given by the P-T conditions deduced for the metapelites intercalated with the calc-silicate rocks and marbles (Soto et al., Chap. 19, this volume). According to these authors, the main assemblage in the metapelites (assemblage 2) developed during the formation of the main foliation (S_2) and is formed by biotite + sillimanite + K-feldspar + plagioclase ± garnet + quartz. The metamorphic evolution these rocks underwent is characterized by a drop in pressure at probably constant or slightly increasing temperatures, which achieved, at the end of the growth of assemblage 2, temperatures of $650 \pm 50^\circ\text{C}$ and pressures of 3–4 kbar. Taking this into account, we calculated the phase relationships at constant temperature conditions ($T = 650^\circ\text{C}$) to estimate the influence of other intensive variables, in particular, pressure.

We present a P- X_{CO_2} phase diagram projection in Figure 8, calculated using the Vertex computing method of Connolly (1990) and the chemical system $\text{Al}_2\text{O}_3\text{-FeO-MgO-Na}_2\text{O-fluid (H}_2\text{O-CO}_2\text{)}$. In the calculated diagram (Figs. 8A, 8B) we represent phase relationships including garnet, clinopyroxene, amphibole, clinozoisite, and plagioclase, after projecting through the saturated components and phases SiO_2 (quartz) and CaO (calcite). In Figure 8A, only the univariant reactions of interest were represented, together with the wollastonite-in and the titanite-out reactions, also calculated and superposed in the diagram. In this figure, the stability field of the observed assemblage is loosely constrained to the area where titanite and anorthite are stable, and clinozoisite and wollastonite are not stable. P- X_{CO_2} conditions can be constrained more precisely in the enlarged window shown in Figure 8B, where the high-variance reactions are also represented. These curves are actually isopleths that contour the anorthite content in plagioclase (long, dashed curves) and the grossular content of garnet (thin, solid curves). The reaction of clinopyroxene to amphibole is also represented (short, dashed curves); its position depends on plagioclase composition. Coexisting plagioclase, garnet, clinopyroxene, and amphibole, with compositions similar to those observed in the studied rock, are stable in the field between 7.4 and 8.2 kbar for X_{CO_2} values between 0.11 and 0.16 (shaded area in Fig. 8B). The high-pressure limit for this assemblage is imposed by the univariant reaction defining the stability field of the clinozoisite + amphibole assemblage, which is not found in these rocks. At pressures <7.4 kbar, coexisting garnet, clinopyroxene, and plagioclase are no longer stable (thick dashed curve in Fig. 8B). Instead, and in good agreement with textural observations, the breakdown reaction of clinopyroxene to amphibole occurs in the presence of an anorthite-rich plagioclase. In Figure 8B, the disappearance of clinopyroxene would occur along a high-variance reaction with decreasing P and increasing X_{CO_2} (shaded arrow). Other possible paths that would produce amphibole at the expense of clinopyroxene, for example, a decreasing P path at constant X_{CO_2} , can be discarded because they would produce a plagioclase richer in Na than that observed here.

Phase relationships were not calculated for the scapolite-bearing rocks because of the lack of available thermodynamic data for the mizzonite end-member and the great uncertainties in the theoretically calculated data for this phase. Nevertheless, several estimations about mizzonite stability conditions can be obtained by comparing these scapolites with the composition of others reported in the literature. The stability field of scapolite with respect to plagioclase and calcite is essentially controlled by temperature: Na extends its stability field toward lower temperatures (Goldsmith and Newton, 1977). According to Abart (1995), and references therein, mizzonite chemical composition requires minimum temperatures of 550°C . This is in agreement with conditions estimated by other authors for calc-silicate rocks with scapolites similar to those reported in this work: 600°C (Motoyoshi et al., 1991) and 550°C (Droop and Al-Filali, 1996). In summary, we can suggest that the scapolite presented in this

work probably grew at temperatures of around $550^\circ\text{--}600^\circ\text{C}$ and an undetermined pressure. These temperature conditions could explain the observed growth of scapolite surrounding clinopyroxene grains.

CONCLUSIONS

Two main groups of mineral assemblages can be distinguished in the calc-silicate rocks of the Alboran metamorphic basement (Holes 976B and 976E) on the basis of the presence of garnet or scapolite. Garnet-bearing rocks display a sequence of up to seven textural and compositional zones with different high-variance mineral assemblages. These zones are interpreted to have formed because of diffusional processes (mainly transfer of CaO) between adjacent impure calcite-bearing marble and aluminum-rich metapelites. The most representative assemblage, in the contact between two reaction zones, is formed by grossular-rich garnet + clinopyroxene + amphibole + plagioclase and was probably stable at $T \sim 650^\circ\text{C}$, $P = 7.4\text{--}8.2$ kbar and $X_{\text{CO}_2} = 0.11\text{--}0.16$, as suggested by phase-relationship analysis. Secondary actinolitic amphibole probably developed in decreasing P and increasing X_{CO_2} conditions. The other type of calc-silicate rocks, scapolite-bearing rocks, grew at similar or slightly lower temperature and an undetermined pressure.

These metamorphic conditions compare well with those deduced by Soto et al. (Chap. 19, this volume) for the high-grade metapelites intercalated with the calc-silicate rocks and also with the P-T conditions deduced for metapelites in different units of the Alpujarride Complex from the Betic chain (see Monié et al., 1994; and Sánchez-Gómez et al., Chap. 23, this volume, for a review). Therefore, this paper demonstrates that phase-relationship analysis of reaction zones formed along metapelite-marble contacts can be a powerful tool contributing to understanding the metamorphic evolution of the Alboran Basement.

ACKNOWLEDGMENTS

J.I. Soto acknowledges ODP for inviting him to participate in Leg 161. We would also like to thank the Shipboard Scientific Party, the ODP technicians, and the SEDCO drilling crew of Leg 161 for their help, and Menchu Comas, one of the Co-Chief Scientists, for her support. We are indebted to Rainer Abart and Bernardo Cesare for their constructive reviews and suggestions. We also thank Christine Laurin for her revision of the English text and Phyllis M. Garman for editorial comments. Financial support was provided by Projects AMB95-1775-CICYT, and AMB95-0535.

REFERENCES

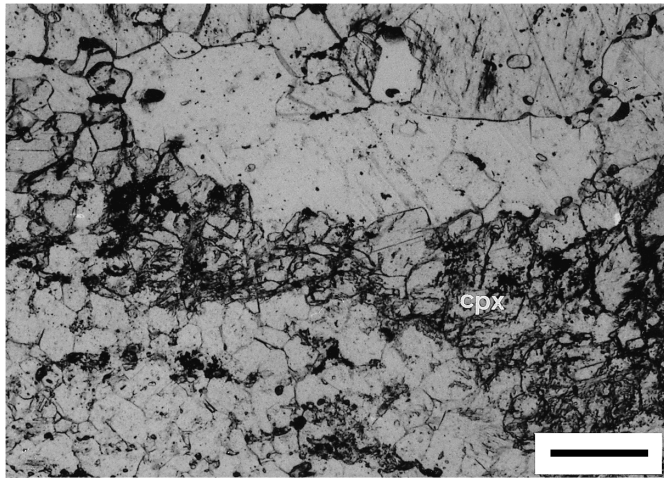
- Abart, R., 1995. Phase equilibrium and stable isotope constraints on the formation of metasomatic garnet-vesuvianite veins (SW Adamello, N Italy). *Contrib. Mineral. Petrol.*, 122:116–133.
- Berman, R.G., 1990. Mixing properties of Ca-Mg-Fe-Mn garnets. *Am. Mineral.*, 75:328–344.
- Brady, J.B., 1977. Metasomatic zones in metamorphic rocks. *Geochim. Cosmochim. Acta*, 41:113–125.
- Comas, M.C., García-Dueñas, V., and Jurado, M.J., 1992. Neogene tectonic evolution of the Alboran Basin from MCS data. *Geo-Mar. Lett.*, 12:157–164.
- Comas, M.C., García-Dueñas, V., Soto, J.I., and Campos, J., 1993. An extensional basin developed on a collisional orogen: the Alborán Sea. In Seranne, M., and Malavielle, J. (Eds.), *Late Orogenic Extension in Mountain Belts*. Doc. B.R.G.M. Fr., 219:44–46.
- Comas, M.C., Zahn, R., Klaus, A., et al., 1996. *Proc. ODP, Init. Repts.*, 161: College Station, TX (Ocean Drilling Program).
- Connolly, J.A.D., 1990. Multivariable phase diagrams: an algorithm based on generalized thermodynamics. *Am. J. Sci.*, 290:666–718.

- de la Linde, J., Comas, M.C., and Soto, J.I., 1996. Morfología del basamento en el nor-oeste del Mar de Alborán. *Geogaceta*, 20:355–358.
- Droop, G.T.R., and Al-Filali, I.Y., 1996. Interaction of aqueous fluids with calcareous metasediments during high-T, low-P regional metamorphism in the Qadda area, southern Arabian Shield. *J. Metamorph. Geol.*, 14:613–634.
- García-Dueñas, V., Balanyá, J.C., and Martínez-Martínez, J.M., 1992. Miocene extensional detachments in the outcropping basement of the northern Alboran basin (Betics) and their tectonic implications. *Geo-Mar. Lett.*, 12:88–95.
- Goldsmith, J.R., and Newton, R.C., 1977. Scapolite-plagioclase stability relations at high pressure and temperatures in the system $\text{NaAlSi}_3\text{O}_8\text{-CaAl}_2\text{Si}_2\text{O}_8\text{-CaCO}_3\text{-CaSO}_4$. *Am. Mineral.*, 62:1063–1081.
- Holland, T.J.B., and Powell, R., 1990. An enlarged and updated internally consistent dataset with uncertainties and correlations: the system $\text{K}_2\text{O-Na}_2\text{O-CaO-MgO-MnO-FeO-Fe}_2\text{O}_3\text{-Al}_2\text{O}_3\text{-TiO}_2\text{-SiO}_2\text{-C-H}_2\text{-O}_2$. *J. Metamorph. Geol.*, 8:89–124.
- Joesten, R., 1977. Evolution of mineral assemblage zoning in diffusion metasomatism. *Geochim. Cosmochim. Acta*, 41:649–670.
- , 1991. Local equilibrium in metasomatic processes revisited: diffusion-controlled growth of chert nodule reaction rims in dolomite. *Am. Mineral.*, 76:743–755.
- Kerrick, D.M., 1977. The genesis of zoned skarns in the Sierra Nevada, California. *J. Petrol.*, 18:144–181.
- Kretz, R., 1983. Symbols for rock-forming minerals. *Am. Mineral.*, 68:277–279.
- Leake, B.E., 1978. Nomenclature of amphiboles. *Can. Mineral.*, 16:501–520.
- Monié, P., Torres-Roldán, R.L., and García-Casco, A., 1994. Cooling and exhumation of the western Betic Cordilleras, $^{40}\text{Ar}/^{39}\text{Ar}$ thermochronological constraints on a collapsed terrane. *Tectonophysics*, 238:353–379.
- Motoyoshi, Y., Thost, D.E., and Hensen, B.J., 1991. Reaction textures in calc-silicate granulites from the Bolingen Islands, Prydz Bay, East Antarctica: implications for the retrograde P–T path. *J. Metamorph. Geol.*, 9:293–300.
- Newton, R.C., Charlu, T.V., and Kleppa, O.J., 1980. Thermochemistry of the high structural state plagioclases. *Geochim. Cosmochim. Acta*, 44:933–941.
- Platt, J.P., and Vissers, R.L.M., 1989. Extensional collapse of thickened continental lithosphere: a working hypothesis for the Alboran Sea and Gibraltar Arc. *Geology*, 17:540–543.
- Pouchou, J.L., and Pichoir, F., 1985. PAP $\phi(\rho z)$ procedure for improved quantitative microanalysis. In Armstrong, J.T. (Ed.), *Microbeam Analysis*: (San Francisco Press), 104–106.
- Shipboard Scientific Party, 1973. Western Alboran Basin Site 121. In Ryan, W.B.F., Hsü, K.J., et al., *Init. Repts. DSDP, 13*: Washington (U.S. Govt. Printing Office), 43–89.
- Shipboard Scientific Party, 1996. Site 976. In Comas, M.C., Zahn, R., Klaus, A., et al., *Proc. ODP, Init. Repts.*, 161: College Station, TX (Ocean Drilling Program), 179–297.
- Soto, J.I., Comas, M.C., and de la Linde, J., 1996. Espesor de sedimentos en la cuenca de Alborán mediante una conversión sísmica corregida. *Geogaceta*, 20:382–385.
- Thompson, A.B., 1975. Calc-silicate diffusion zones between marble and pelitic schist. *J. Petrol.*, 16:314–346.
- Thompson, J.B., Jr., 1959. Local equilibrium in metasomatic processes. *Res. Geochem.*, 1:427–457.
- , 1981. An introduction to the mineralogy and petrology of biopyriboles. In Veblen, D.R. (Ed.), *Amphiboles and other Hydrous Pyriboles: Mineralogy*. *Rev. Mineral., Mineral. Soc. Am.*, 9A:141–188.
- Watts, A.B., Platt, J.P., and Buhl, P., 1993. Tectonic evolution of the Alboran Sea Basin. *Basin Res.*, 5:153–177.
- Wood, B.J., and Banno, S., 1973. Garnet-orthopyroxene and orthopyroxene-clinopyroxene relationships in simple and complex systems. *Contrib. Mineral. Petrol.*, 42:109–124.

Date of initial receipt: 7 May 1997

Date of acceptance: 3 November 1997

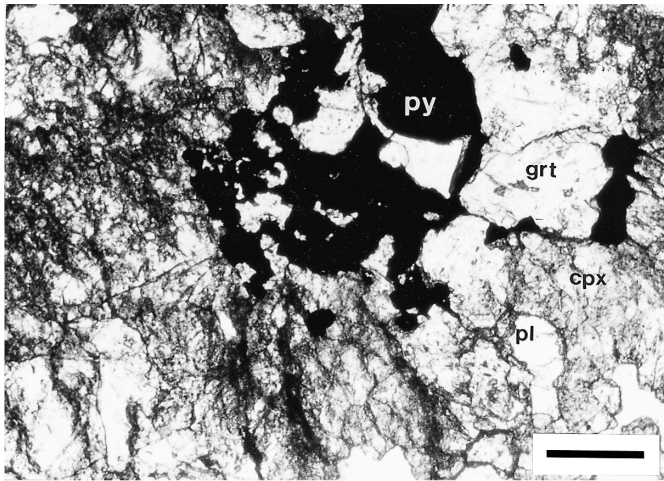
Ms 161SR-217



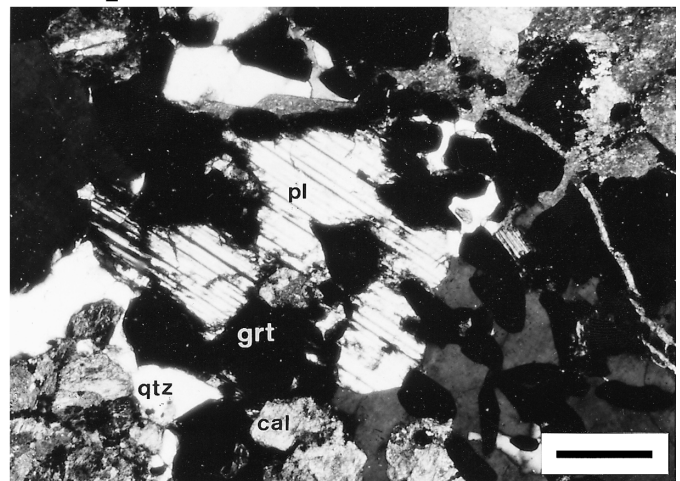
1



2

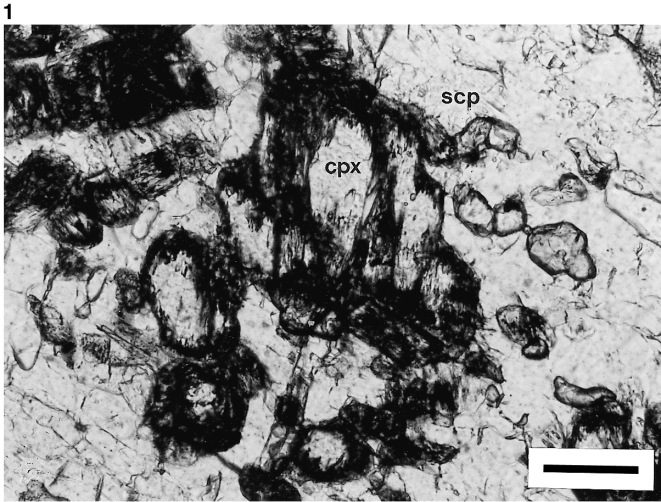
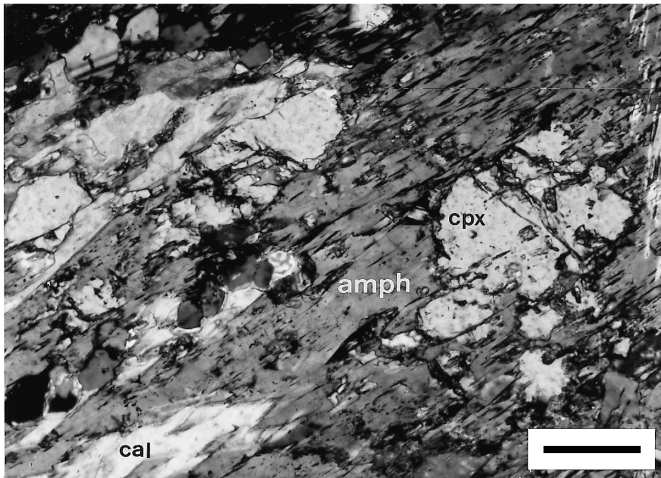


3

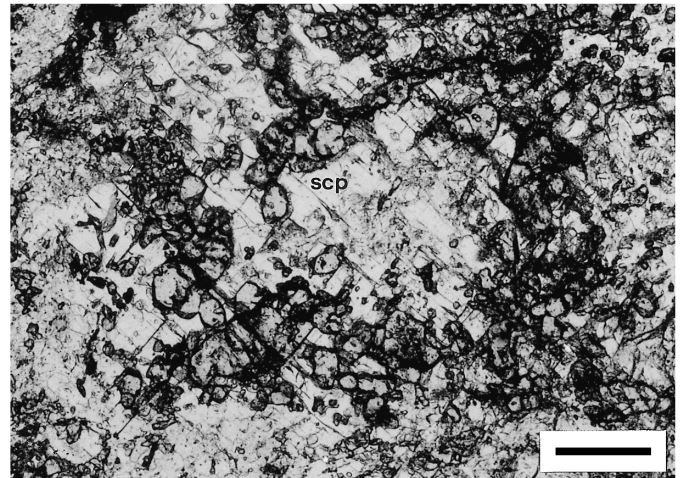


4

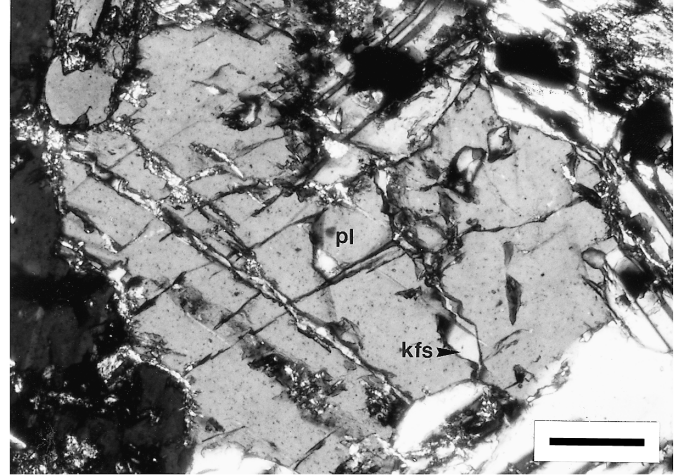
Plate 1. **1.** Clinopyroxene (cpx) band in the contact between marble (upper part) and quartz + feldspar-rich metapelite layers (lower part). Sample 161-976E-15R-3, 35–36 cm. Scale bar is 214 μm . **2.** Band of massive garnet (grt) in the contact between marble (upper part) and metapelite (lower part). Veins in garnet are filled with plagioclase and opaque minerals. Sample 161-976E-21R-3, 27–31 cm. Scale bar is 214 μm . **3.** Coexisting garnet (grt), clinopyroxene (cpx), plagioclase (pl), and pyrite (py) from Zone VI. Sample 161-976B-76R-1, 66–87 cm. Scale bar is 214 μm . **4.** Xenomorphic relics of garnet (grt) after breakdown reaction to plagioclase (pl), calcite (cal), and quartz (qtz). Sample 161-976E-22R-2, 90–94 cm. Scale bar is 85 μm .



1



2



3

4

Plate 2. **1.** Breakdown reaction of clinopyroxene (cpx) to amphibole (amph) and calcite (cal). Sample 161-976B-76R-2, 115–118 cm. Scale bar is 85 μm . **2.** Poikiloblastic scapolite (scp) with inclusions of clinopyroxene. Sample 161-976E-15R-1, 126–128 cm. Scale bar is 214 μm . **3.** Detail of clinopyroxene (cpx) inclusions in large scapolite (scp) poikiloblasts. Clinopyroxene grains are partially or completely replaced by late retrogressive sheet minerals. Sample 161-976E-15R-1, 94–98 cm. Scale bar is 85 μm . **4.** Plagioclase (pl) grains cut by K-feldspar (kfs) veins. Sample 161-976B-104R-1, 59–62 cm. Scale bar is 85 μm .